



Unexpected enhancement of new particle formation by lactic acid sulfate resulting from SO₃ loss in forested and agricultural regions

Rui Wang¹, Shuqin Wei^{1,★}, Zeyao Li^{1,★}, Kaiyu Xue¹, Rui Bai¹, and Tianlei Zhang¹

¹Shaanxi Key Laboratory of Catalysis, School of Chemical & Environment Science, Shaanxi University of Technology, Hanzhong, Shaanxi 723001, China

★These authors contributed equally to this work.

Correspondence: Tianlei Zhang (ztianlei88@163.com)

Received: 3 October 2025 – Discussion started: 29 October 2025

Revised: 15 January 2026 – Accepted: 4 February 2026 – Published: 27 February 2026

Abstract. Organosulfates (OSs) are key components of atmospheric aerosols and serve as tracers for secondary organic aerosol (SOA) formation. Among these, lactic acid sulfate (LAS) has been increasingly detected in the atmosphere. However, its molecular formation pathways and its role in new particle formation (NPF) remain poorly understood. In this work, we investigate the gas-phase formation mechanism of LAS via the reaction between lactic acid (LA) and SO₃, and assess its impact on sulfuric acid-ammonia (SA-A) driven NPF using quantum chemical calculations and Atmospheric Cluster Dynamics Code (ACDC) kinetic modeling. Our results show that SA and H₂O significantly catalyze the LA-SO₃ reaction, enhancing the effective rate coefficient by 7–10 orders of magnitude within the temperature range of 280–320 K. Further molecular-level analysis using the ACDC reveals that LAS not only significantly enhances the clustering stability of SA and A up to 10⁸-fold, but also plays a significant and direct role in SA-A nucleation under conditions typical of forested and agricultural regions. Notably, LAS-SA-A clusters contribute to 97 % of the overall cluster formation pathways in regions with high LAS concentrations like Centreville, Alabama. Additionally, our findings show that the nucleation potential of LAS-SA-A clusters is stronger than that of LA-SA-A clusters, aligning with field observations, even though LAS concentrations are typically three orders of magnitude lower than LA. These findings imply that OSs formed through SO₃ consumption may significantly contribute to the enhanced NPF rates observed in continental regions.

1 Introduction

Atmospheric aerosol particles pose significant risks to public health, adversely affecting both the respiratory and cardiovascular systems (Anderson et al., 2012; Xing et al., 2016; Zhang et al., 2023b). Beyond health implications, these particles contribute to global warming by reducing visibility and disrupting the Earth's radiative balance (Lund et al., 2019; Zheng et al., 2018). As a major source of atmospheric aerosols, new particle formation (NPF), accounts for over 50 % of the total particle number concentration and is strongly associated with severe haze events in megacities

across China (Kulmala et al., 2004; Brean et al., 2020). Despite its significance, accurately characterizing the NPF process remains a considerable challenge, primarily due to limitations in current measurement techniques and an incomplete comprehension of the underlying mechanisms. While field observations and CLOUD chamber experiments (Kulmala et al., 2004; Dai et al., 2023; Lee et al., 2019; Hirsikko et al., 2011; Zhang et al., 2015) have provided valuable insights, they are insufficient to fully elucidate these processes. To address these gaps, a molecular-level approach is essential, as it allows for a more precise understanding of nucleation mechanisms (Yang et al., 2021; Li et al., 2017). This approach

enables the detailed determination of molecular cluster geometries, the strengths of intermolecular interactions, and the pathways of cluster formation (Long et al., 2013; Zu et al., 2024a; Rong et al., 2020a). Such molecular insights are critical to evaluating the impacts of aerosols on the atmosphere and for devising effective strategies to mitigate haze formation.

Gaseous sulfuric acid (SA), derived from the oxidation of SO₂, has long been recognized as a key NPF precursor (Kirkby et al., 2011; Zhao et al., 2024). Molecular-level studies have shown that various nucleation precursors, including water (H₂O) (Zhang et al., 2012b), ammonia (A) (Kirkby et al., 2011; Zhang et al., 2015), methylamine (MA) (Shen et al., 2020), dimethylamine (DMA) (Cai et al., 2021; Kurtén et al., 2008), monoethanolamine (MEA) (Shen et al., 2019), piperazine (PZ) (Ma et al., 2019) and iodic acid (Sipilä et al., 2016), are involved in SA-driven binary nucleation, which serves as a primary initiator of NPF. However, binary nucleation mechanisms alone cannot fully account for the discrepancies observed between measured and modeled global NPF rates (Hodshire et al., 2019; Kirkby et al., 2016), suggesting the involvement of additional gaseous species. Then plenty of low weight molecular organic acids such as glycolic acid (Zhang et al., 2017), malonic acid (Zhang et al., 2018) and pyruvic acid (Tsona Tchinda et al., 2022) also exhibit enhancement effects on ternary nucleation driven by SA-A nucleation system through catalytic mechanisms. Despite recognizing the enhancement provided by SA-A-driven ternary nucleation, the nucleation rates predicted by these mechanisms still fall short when compared to field observations (Kirkby et al., 2016; Hodshire et al., 2019; Yin et al., 2021). The persistent underestimation underscores the need for further investigation into the role of additional gaseous species to better understand the complex mechanisms driving NPF.

Organosulfates (OSs), formed through the chemical transformation of organic acids, constitute a major portion of organosulfur species in atmospheric aerosols, contributing 5%–30% to the organic mass in PM₁₀ (Sun et al., 2025; Brüggemann et al., 2017). These compounds are prevalent in atmospheric particles and are commonly employed as markers to track the formation of secondary organic aerosols (SOAs) in environmental research (Tan et al., 2022; Zhang et al., 2012a; Froyd et al., 2010a; Brüggemann et al., 2017; Mutzel et al., 2015; Glasius et al., 2017). Recent research has led to the identification and characterization of various OSs in fine particulate matter samples from regions including the United States, China, Mexico City and Pakistan (Hettiyadura et al., 2017; Wang et al., 2018; Olson et al., 2011). Meanwhile, studies suggest that the cycloaddition of SO₃ to organic acids could be a key mechanism for OSs formation resulting in compounds with lower vapor pressures than their parent carboxylic acids and increased inter-molecular interaction sites (Smith et al., 2020; Tan et al., 2020; Yao et al., 2020; Zhang et al., 2023a). Notably, lactic acid sulfate (LAS) has been identified as the dominant OSs species

across all these field observations (Darer et al., 2011; Riva et al., 2015; Kundu et al., 2013). However, the specific formation mechanism of LAS from the reaction of lactic acid (LA) with SO₃ remains largely unexplored. Additionally, SA and water (H₂O) (Tan et al., 2022; Zhang et al., 2025; Li et al., 2018b), both prevalent in the atmosphere, act as strong hydrogen atom donors/acceptors, facilitating proton transfer reactions and potentially catalyzing the LA-SO₃ reaction.

The reaction products of SO₃ with major atmospheric trace species have been shown proven to significantly influence the formation of NPF. For instance, compounds such as sulfamic acid (Li et al., 2018a), oxalic sulfuric anhydride (Yang et al., 2021), methyl hydrogen sulfate (Liu et al., 2019), glyoxylic sulfuric anhydride (Rong et al., 2020b) and formic acid sulfate (Wang et al., 2025), generated through reactions of SO₃ with A, oxalic acid, methanol, glyoxylic acid and formic acid, all exhibit catalytic effects on NPF in aerosols. Structurally, LAS, the product of the SO₃+LA reaction, contains both -COOH and -SO₃H functional groups, which facilitate additional hydrogen bonding with atmospheric particle precursors (Yao et al., 2020). However, the role of LAS in enhancing SA-A nucleation remains underexplored, limiting our ability to comprehensively evaluate its impact on NPF processes. Furthermore, LA, a highly oxidized α -hydroxy acid with both -OH and -COOH groups (Mochizuki et al., 2019), can enhance the stability of SA-A clusters and facilitate NPF (Li et al., 2017). Given its relatively larger atmospheric concentrations, particularly in regions with elevated organic acid pollution, LA may also significantly influence NPF. So, understanding the distinct contributions of LAS and LA to SA-A nucleation is crucial, as this will advance our understanding of NPF events, particularly in agricultural and forested regions.

In this work, we utilized quantum chemical calculations together with master equation analysis to investigate the gas-phase reaction of SO₃ with LA that forms LAS, with H₂O and SA serving as catalysts. The role of LAS in enhancing SA-A nucleation was then explored by examining the formation mechanisms of the (LAS)_x(SA)_y(A)_z ($0 \leq z \leq x + y \leq 3$) system using the Atmospheric Clusters Dynamic Code (ACDC) kinetic model. Additionally, the potential influence of LAS on atmospheric new particle formation (NPF) was assessed across diverse global regions. Finally, a comparative study of LA and LAS was also conducted to elucidate the respective roles of organic acids and OSs in enhancing SA-A nucleation, focusing on the formation mechanisms of both LA-SA-A and LAS-SA-A systems.

2 Methodology

2.1 Quantum chemical calculations

The gas-phase reaction of SO₃ with LA to form LAS, both in the absence and presence of H₂O and SA as catalysts, was systematically optimized and calculated using

the Gaussian 09 program (Faloona et al., 2009) at the M06-2X/6-311++G(2df,2pd) level (Stewart, 2007; Walker et al., 2013). Intrinsic reaction coordinate analyses (Hratchian and Schlegel, 2005) were carried out at the same computational level to verify the connection between transition states and their respective pre-reactive complexes and products. Furthermore, single-point energy calculations were refined at the CCSD(T)-F12/cc-pVDZ-F12 level with the ORCA program (Neese, 2012), employing the optimized geometries as input.

To identify the global minimum energy configurations of (SA)_x(A)_y(LAS)_z clusters (where $0 \leq y \leq x+z \leq 3$), we utilized the ABCluster program (Zhang and Dolg, 2016) to systematically generate initial structures for various clusters combinations. Specifically, using the ABCluster procedure and the CHARMM force field, a diverse set of initial structures $n \times 1000$ ($1 \leq n \leq 3$) were randomly produced. Initially, the primary structures were optimized and their energies were ranked using the PM6 method in MOPAC 2016 (Partanen et al., 2016; Stewart, 2007). After the initial sampling, considering the excellent performance of the M06-2X method in accurately characterizing the geometries of atmospheric clusters (Walker et al., 2013; Lu et al., 2020), up to 1000 favorable configurations were selected for rigorous re-optimization at the M06-2X/3-21G* level of theory. Subsequently, the 100 lowest-energy configurations were further optimized using the M06-2X/6-31G(d, p) level of theory, from which the 10 configurations with the lowest energies were identified. Finally, to accurately determine the global minimum, the M06-2X/6-311++G(2df, 2pd) method was applied to refine these 10 lowest-energy configurations.

2.2 Rate coefficients calculations

Rate constants for the SO₃+LA reaction, both without and with H₂O and H₂SO₄ as catalysts, were determined via Rice-Ramsperger-Kassel-Marcus (RRKM) theory (Glowacki et al., 2012; Wardlaw and Marcus, 1984) within the Master Equation (ME/RRKM) framework in MESMER (Master Equation Solver for Multi-Energy Well Reactions) code (Glowacki et al., 2012; Klippenstein and Marcus, 1988). Specifically, in the MESMER calculations, the rate constants for the barrierless formation of pre-reactive complexes from reactants were determined using the Inverse Laplace Transform (ILT) method (Horváth et al., 2020), whereas the subsequent conversion of these complexes to products via transition states was evaluated using RRKM theory (Mai et al., 2018). The ILT method and RRKM theory can be represented in Eqs. (1) and (2), respectively:

$$k^\infty(\beta) = \frac{1}{Q(\beta)} \int_0^\infty k(E) \rho(E) \exp(-\beta E) dE \quad (1)$$

$$k(E) = \frac{W(E - E_0)}{h\rho(E)} \quad (2)$$

Here, h represents Planck's constant, $\rho(E)$ indicates the density of accessible states for the reactant at energy E , E_0 is the reaction threshold energy and $W(E - E_0)$ refers to the rovibrational states of the transition state, excluding motion along the reaction coordinate. Geometries, vibrational frequencies, and rotational constants were obtained at the M06-2X/6-311++G(2df,2pd) level, with single-point energies refined at the method of CCSD(T)-F12/cc-pVDZ-F12.

2.3 ACDC kinetics simulation

The ACDC was utilized to investigate the molecular-level collision coefficient (β , cm³ s⁻¹), evaporation coefficient (γ , s⁻¹) and cluster formation rates (J , cm⁻³ s⁻¹). Thermodynamic parameters and structural information for cluster formation, obtained from quantum chemical calculations performed by M06-2X/6-311++G(2df,2pd), served as input parameters for the ACDC model. The MATLAB-R2014a platform, leveraging its ode15s solver (Shampine and Reichelt, 1997), performed numerical integration of the birth-death equation for the ACDC model, thereby elucidating the kinetics of cluster growth over time. The general form of the birth-death equation for the concentration c_i of cluster i given by,

$$\frac{dc_i}{dt} = \frac{1}{2} \sum_{j < i} \beta_{j,(i-j)} c_j c_{(i-j)} + \sum_j \gamma_{(i+j) \rightarrow i} c_{i+j} - \sum_j \beta_{i,j} c_i c_j - \frac{1}{2} \sum_{j < i} \gamma_{i \rightarrow j} c_i + Q_i - S_i \quad (3)$$

In this formulation, $\beta_{i,j}$ corresponds to the collision frequency factor between clusters of sizes i and j , $\gamma_{(i+j) \rightarrow i}$ quantifies the fragmentation rate of composite clusters into their constituent monomers i and j . The system's open nature is accounted for through Q_i , representing the external flux of cluster i , and S_i , characterizing its removal rate. Sensitivity tests were conducted by varying the condensation sink (Cs) from 6×10^{-4} – 6×10^{-2} s⁻¹, indicating that the Cs exerted minimal influence on the main conclusions (Fig. S11). Therefore, the Cs was set to a representative value of 2.6×10^{-3} for all subsequent calculations (Liu et al., 2021). Additionally, (LAS)₄(A)₃, (LAS)₄(A)₄, (LAS)₂(SA)₂(A)₃, (LAS)₂(SA)₂(A)₄, (LAS)(SA)₃(A)₃, (LAS)(SA)₃(A)₄, (SA)₄(A)₃ and (SA)₄(A)₄ clusters are acting as boundary clusters for LAS-SA-A system. Also, the details of the contribution of LAS to SA-A nucleation was estimated in the first part of the Supplement.

3 Results and discussions

3.1 Formation of LAS via the reaction of SO₃ with LA

In the direct cycloaddition pathway (Channel LAS) illustrated in Fig. 1, the hydroxyl (-OH) group of LA reacts with the sulfur atom of SO₃, leading to the formation of LAS

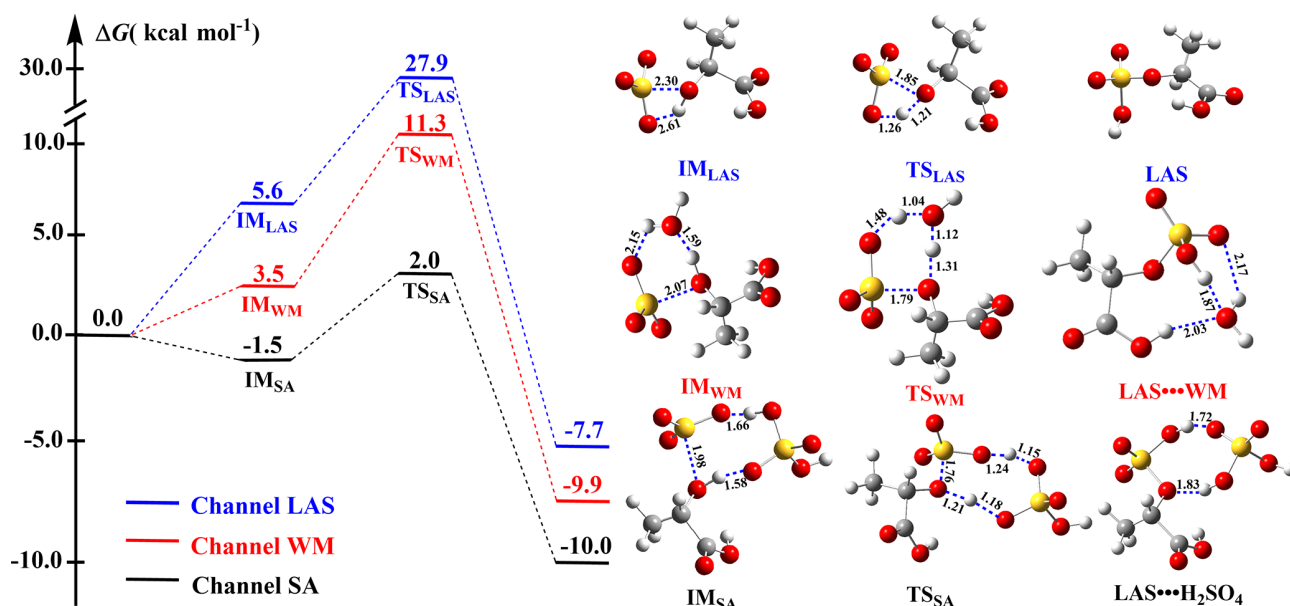


Figure 1. Potential energy profiles and corresponding molecular structures for the $\text{LA} + \text{SO}_3 \rightarrow \text{LAS}$ reaction in the absence and presence of H_2O and H_2SO_4 investigated at the CCSD(T)-F12/cc-pVDZ-F12/M06-2X/6-311++G(2df,2pd) level.

via proton transfer from LA to SO_3 . However, the resulting $\text{SO}_3 \cdots \text{LA}$ complex (denoted as IM) is thermodynamically unstable, primarily due to the significant ring strain in the four-membered structure, exhibiting a relative Gibbs free energy of $5.6 \text{ kcal mol}^{-1}$. The Gibbs free energy barrier for this reaction is calculated to be $22.3 \text{ kcal mol}^{-1}$. As indicated in Table S5, the rate coefficients for Channel LAS are extremely low, spanning from 1.35×10^{-26} to $6.21 \times 10^{-25} \text{ cm}^3 \text{ molecule}^{-1} \text{ s}^{-1}$ across the temperature range of 230–320 K. These values suggest that this pathway is both slow and thermodynamically unfavorable for LAS formation under typical atmospheric conditions.

H_2O , highly abundant in the atmosphere with concentration around $10^{17} \text{ molecules cm}^{-3}$ (Huang et al., 2015), serves as both a donor and acceptor of hydrogen bonds, and is widely recognized for its ability to catalyze a wide range of proton transfer reactions. To assess its catalytic effect on the formation of LAS, we examined the $\text{SO}_3 + \text{LA}$ reaction in the presence of H_2O (Channel WM), as illustrated in Fig. 1. This reaction can proceed via three possible sequential bimolecular pathways: (i) $\text{SO}_3 \cdots \text{LA} + \text{H}_2\text{O}$, (ii) $\text{SO}_3 \cdots \text{H}_2\text{O} + \text{LA}$ and (iii) $\text{LA} \cdots \text{H}_2\text{O} + \text{SO}_3$. Considering typical atmospheric concentrations of SO_3 ($10^5 \text{ molecules cm}^{-3}$) (Zhang et al., 2024), LA ($10^{12} \text{ molecules cm}^{-3}$) (Li et al., 2017) and H_2O ($10^{17} \text{ molecules cm}^{-3}$) (Huang et al., 2015), the calculated concentrations of $\text{SO}_3 \cdots \text{LA}$, $\text{SO}_3 \cdots \text{H}_2\text{O}$ and $\text{LA} \cdots \text{H}_2\text{O}$ complexes at 298 K are 4.18×10^{-2} , 5.80×10^3 and $2.32 \times 10^8 \text{ molecules cm}^{-3}$, respectively (see Table S2 in the Supplement). These results suggest that Channel WM predominantly proceeds via the collision of $\text{LA} \cdots \text{H}_2\text{O}$ with SO_3 .

The free energy barrier for Channel WM is $7.8 \text{ kcal mol}^{-1}$, which is $14.5 \text{ kcal mol}^{-1}$ lower than the barrier for the uncatalyzed cycloaddition pathway. At the experimental concentration of H_2O ($[\text{H}_2\text{O}] = 10^{17} \text{ molecules cm}^{-3}$) (Huang et al., 2015), the effective rate coefficient for the H_2O -catalyzed reaction is $2.00 \times 10^{-16} \text{ cm}^3 \text{ molecule}^{-1} \text{ s}^{-1}$, which is nine orders of magnitude greater than the rate for the direct cycloaddition pathway ($2.22 \times 10^{-25} \text{ cm}^3 \text{ molecule}^{-1} \text{ s}^{-1}$). These results clearly demonstrate that the H_2O -catalyzed $\text{LA} + \text{SO}_3$ reaction represents a significantly more favorable route for LAS formation. Detailed effective rate coefficients for the H_2O -catalyzed reaction are provided in Fig. 2a.

SA is another abundant atmospheric species that efficiently donates and accepts hydrogen bond, facilitating proton transfer (Yao et al., 2018; Tan et al., 2018) and potentially catalyzing the $\text{LA} + \text{SO}_3$ reaction. As shown in Fig. 1, SA is significantly more effective than H_2O in promoting LAS formation via cycloaddition. Specifically, SA increases the stabilization energy of the $\text{SO}_3 \cdots \text{LA}$ complex by $7.1 \text{ kcal mol}^{-1}$, $5.0 \text{ kcal mol}^{-1}$ greater than the stabilization provided by H_2O and reduces the distance between the oxygen atom of the $-\text{OH}$ group in LA and the sulfur atom in SO_3 by 0.09 \AA in the $\text{SO}_3 \cdots \text{LA} \cdots \text{SA}$ complex. As compared with six-membered ring transition state TS_{WM} , the transition state TS_{SA} shows eight-membered ring structure, which reduces the ring tension greatly. So, from an energetic point of view, SA lowers the Gibbs free energy barrier to $3.5 \text{ kcal mol}^{-1}$, $4.3 \text{ kcal mol}^{-1}$ lower than the barrier observed for the H_2O -catalyzed pathway. The effective rate coefficients for the SA ($[\text{SA}] = 10^7 \text{ molecules cm}^{-3}$)-catalyzed reaction (k_{SA}) is 4–5 orders of magnitude higher than that for the H_2O -catalyzed

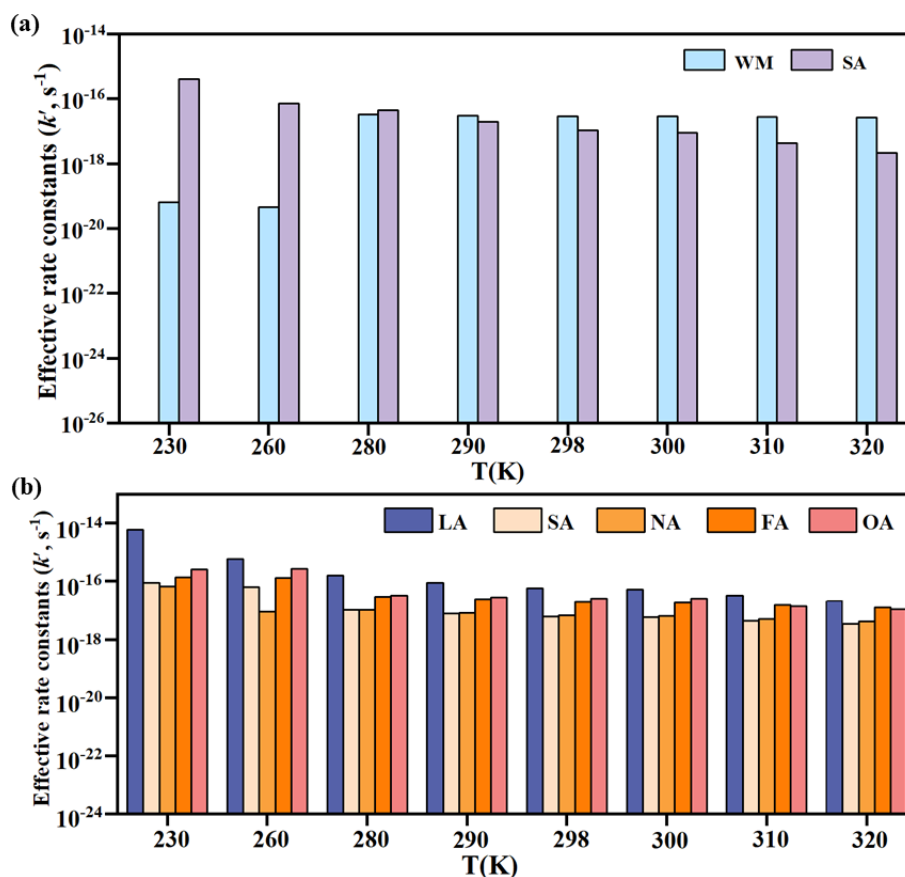


Figure 2. (a) Effective rate constants for the $\text{LA} + \text{SO}_3 \rightarrow \text{LAS}$ reaction in the presence of H_2O (k'_{WM} , $\text{cm}^3 \text{molecule}^{-1} \text{s}^{-1}$) and H_2SO_4 (k'_{SA} , $\text{cm}^3 \text{molecule}^{-1} \text{s}^{-1}$) calculated using the master equation over the temperature range of 230–320 K; (b) Effective rate constants (k' , s^{-1}) for the hydrolysis of SO_3 with various species X ($X = \text{LA}, \text{SA}, \text{NA}, \text{FA}$ and OA) within the temperature range of 230–320 K, where SA, NA, FA and OA are denoted as H_2SO_4 , HNO_3 , HCOOH and $\text{H}_2\text{C}_2\text{O}_4$, respectively.

pathway (k'_{WM}) at 100% relative humidity, indicating that SA is kinetically more favorable, particularly at altitudes of 5–10 km. Thus, SA predominantly catalyzes the $\text{SO}_3 + \text{LA}$ reaction, significantly contributing to the gas-phase loss of SO_3 in LA-rich atmospheric regions.

Previous theoretical studies have indicated that atmospheric acids can catalyze the hydrolysis of SO_3 to form SA (Hazra and Sinha, 2011; Cheng et al., 2022; Long et al., 2013; Lv et al., 2019). In this context, the potential catalytic role of LA in SO_3 hydrolysis was also explored. The potential energy surface (PES) for this reaction is presented in Fig. S2, with the effective rate coefficients compared to those for SO_3 hydrolysis catalyzed by SA, HNO_3 , HCOOH , and OA. As shown in Fig. 2b, LA predominantly catalyzes SO_3 hydrolysis within the temperature range of 280–320 K at a concentration of $1.0 \times 10^{12} \text{molecules cm}^{-3}$. Besides, given the current lack of atmospheric field data on gas-phase LAS and lactic acid sulfuric anhydride (LASA, the product from the reaction between SO_3 and the carboxyl group of LA, Fig. S1), thermodynamic equilibrium calculations were used to estimate their concentrations and assess their poten-

tial impacts on atmospheric NPF. Modeling results suggest LAS concentrations of 10^3 – $10^5 \text{molecules cm}^{-3}$, which is nine orders of magnitude higher than that of LASA (ranging from 10^{-6} – $10^{-4} \text{molecules cm}^{-3}$). This suggests that LAS has significantly more atmospheric relevance than LASA, with a correspondingly higher potential to influence NPF. Detailed calculations and further insights are provided in Table S4.

3.2 Enhancing effect of LAS on SA-A-driven NPF

The role of LAS in promoting SA-A-driven NPF process was thoroughly examined. Initially, potential interaction sites between LAS and SA-A clusters were identified through molecular analyses. Next, the stable structures and thermodynamic stabilities of various $(\text{LAS})_x(\text{SA})_y(\text{A})_z$ ($y \leq x+z \leq 3$) clusters were characterized, providing insight into their structural integrity. Building on these findings, the nucleation mechanism of the SA-A-LAS system was investigated, with a particular focus on the impact of temperature and precursor concentrations on LAS-mediated NPF processes. Finally,

the atmospheric implications of LAS-enhanced SA-A nucleation were evaluated, especially in forested and agricultural-developed regions.

3.2.1 Cluster stability analysis

Stable cluster formation is primarily driven by strong interactions between nucleation precursors (Lu and Chen, 2012). To assess the binding potential of LAS with the SA-A cluster, the electrostatic potential (ESP)-mapped molecular van der Waals surface was calculated to identify key interaction sites. As shown in Fig. 3, the hydrogen atom of the $-\text{SO}_3\text{H}$ moiety in LAS exhibits a positive ESP of $+78.73 \text{ kcal mol}^{-1}$, suggesting its role as a hydrogen bond donor that can interact with the double-bonded oxygen atom of SA or the nitrogen atom of A, both of which act as hydrogen bond acceptors. Additionally, the double-bonded oxygen in LAS, with a negative ESP of $-32.51 \text{ kcal mol}^{-1}$, can act as a hydrogen-bond acceptor, interacting with the hydroxyl hydrogen of SA ($-\text{OH}$) or the hydrogen of A. These intermolecular interactions imply that LAS enhances nucleation efficiency between SA and A during aerosol nucleation, thereby stabilizing the resulting molecular clusters. Based on the ESP analysis, the most stable configurations of $(\text{LAS})_x(\text{SA})_y(\text{A})_z$ ($z \leq x+y \leq 3$) clusters were identified (Fig. S3), with the observed interaction sites in the ternary clusters corresponding well to the ESP predictions.

To quantitatively evaluate the binding strength of LAS within binary SA-A-based clusters, the Gibbs free energies (ΔG , kcal mol^{-1} , Table S7) for the $(\text{LAS})_x(\text{SA})_y(\text{A})_z$ ($z \leq x+y \leq 3$) clusters were calculated at temperatures of 238.15, 258.15, 278.15 and 298.15 K. All clusters exhibited negative ΔG values, confirming thermodynamic favorability. Importantly, ternary SA-A-LAS clusters consistently demonstrated lower ΔG values compared to their binary counterparts, suggesting that the presence of LAS reinforces the stability of SA-A clusters. Further analysis of stability at 278.15 K was carried out by examining total evaporation rates ($\sum \gamma$), derived from cluster ΔG values (Table S7) and collision rates (β , Table S8), as summarized in Fig. 4. Previous research indicates that lower $\sum \gamma$ are indicative of greater cluster stability (Li et al., 2024; Zu et al., 2024b). At 278.15 K, clusters incorporating LAS exhibit a lower $\sum \gamma$ compared to those composed solely of SA and A molecules. For example, the $\sum \gamma$ values for the $(\text{A})_1 \cdot (\text{LAS})_1$ ($1.19 \times 10^4 \text{ s}^{-1}$) and $(\text{A})_3 \cdot (\text{LAS})_3$ ($8.64 \times 10^{-8} \text{ s}^{-1}$) clusters were $3.1\text{--}10^8$ times lower than those for the $(\text{SA})_1 \cdot (\text{A})_1$ ($3.73 \times 10^4 \text{ s}^{-1}$) and $(\text{SA})_3 \cdot (\text{A})_3$ ($3.28 \times 10^1 \text{ s}^{-1}$) clusters. Similarly, the $\sum \gamma$ values of the $(\text{SA})_1 \cdot (\text{A})_3 \cdot (\text{LAS})_2$ ($1.99 \times 10^0 \text{ s}^{-1}$) and $(\text{SA})_2 \cdot (\text{A})_3 \cdot (\text{LAS})_1$ ($2.29 \times 10^{-4} \text{ s}^{-1}$) clusters at 278.15 K were found to be $10^1\text{--}10^5$ times lower than the most stable binary cluster, $(\text{SA})_3 \cdot (\text{A})_3$ ($3.28 \times 10^1 \text{ s}^{-1}$). Moreover, these clusters exhibited $\beta C / \sum \gamma$ ratios greater than 1 (Table S11), suggesting a favorable balance between cluster growth and evaporation. Similar trends in ΔG and

$\sum \gamma$ were observed across the other temperatures studied, including 238.15, 258.15 and 298.15 K. Taken together, the ΔG and $\sum \gamma$ analyses provide strong evidence that LAS incorporation enhances SA-A cluster stability, thereby increasing their likelihood of participating in nucleation events.

3.2.2 Cluster formation pathways

To investigate the detailed nucleation pathways of LAS in the formation of SA-A clusters, ACDC simulation were conducted at 278.15 K, with the concentrations of [SA] ($10^6 \text{ molecules cm}^{-3}$), [A] ($10^9 \text{ molecules cm}^{-3}$) and [LAS] ($10^5 \text{ molecules cm}^{-3}$). The results are presented in Fig. 5a, illustrating two distinct mechanisms for cluster growth. The first pathway (depicted by black arrows) corresponds to pure SA-A clustering, starting from the $(\text{SA})_1 \cdot (\text{A})_1$ dimer. Subsequent stepwise addition of SA or A monomers drives the assembly of progressively larger and more stable clusters such as $(\text{SA})_3 \cdot (\text{A})_3$, which eventually exit the system. The second pathway (depicted by blue arrows) includes clusters containing LAS, in which LAS performs two distinct roles: one as a “catalyst” and the other as a “participant”. When LAS acts as a “catalyst”, the $(\text{SA})_1 \cdot (\text{A})_2 \cdot (\text{LAS})_1$ trimer collides with the SA monomer, forming the $(\text{SA})_2 \cdot (\text{A})_2 \cdot (\text{LAS})_1$ cluster. Subsequently, LAS evaporates from the cluster, leaving behind the $(\text{SA})_2 \cdot (\text{A})_2$ cluster. Meanwhile, when LAS acts as a “participant”, collisions between the $(\text{SA})_1 \cdot (\text{A})_1$ dimer and LAS monomers lead to the assembly of the $(\text{SA})_1 \cdot (\text{A})_1 \cdot (\text{LAS})_1$ cluster. This trimer then undergoes further collisions with either an SA or A monomer, producing the $(\text{SA})_2 \cdot (\text{A})_3 \cdot (\text{LAS})_1$ cluster, which ultimately grows out of the system. These dual roles of LAS in SA-A clusters are observed across other temperatures of 298.15, 238.15 and 258.15 K; however, at lower temperatures, such as 238.15 K, the LAS-involved pathway simplifies (as shown in Figs. S8, S9 and S10).

As shown in Fig. 5b, the contributions of LAS to the SA-A nucleation process were examined across a range of temperatures, with a focus on the nucleation mechanism that involves LAS participation. As temperature increases, the influence of LAS-involved pathways becomes progressively more dominant, due to the elevated vapor pressure of LAS raises its gas-phase concentration, thereby promoting further cluster formation. At lower temperatures (238.15 and 258.15 K), SA-A clustering remains the dominant process, accounting for 73 % of nucleation events, while LAS-involved pathways contribute a modest 21 %, because of the reduced collision frequency of LAS. However, as the temperature rises to 278.15 K, LAS participation increases to 33 %, signaling a more prominent role in cluster growth. At 298.15 K, this contribution further rises to 49 %, nearly double that observed at the lower temperatures. These results highlight the crucial role of elevated temperatures in enhancing LAS’s contribution to SA-A nucleation, emphasizing the temperature-dependent amplification of LAS-driven cluster formation.

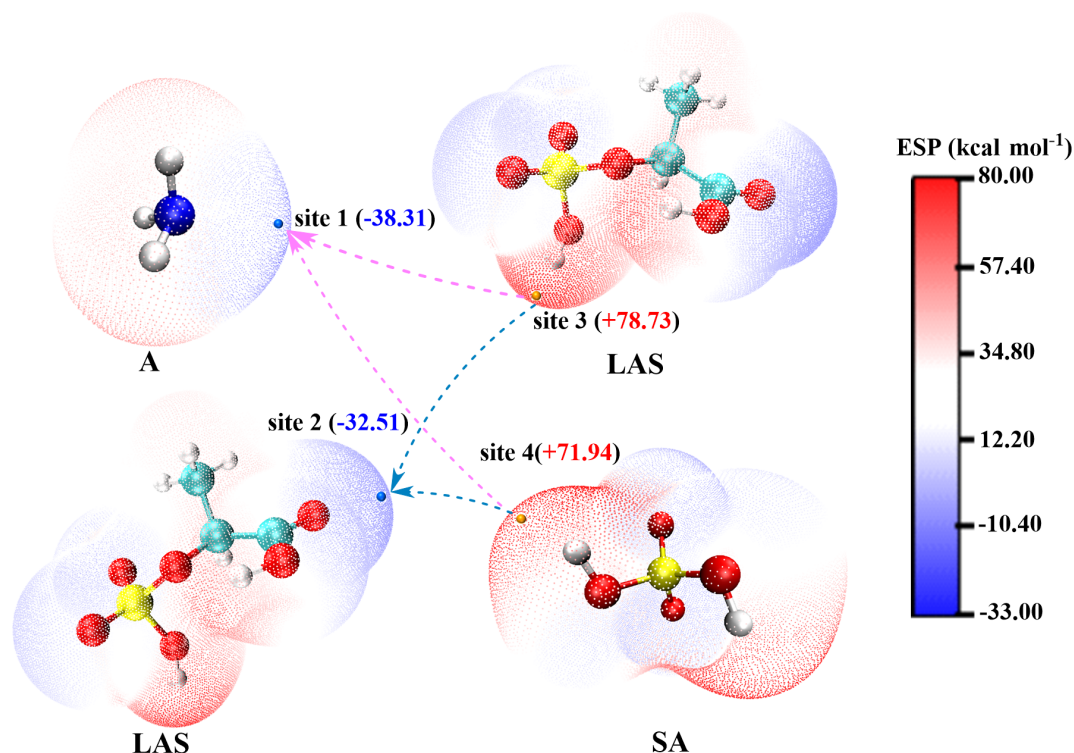


Figure 3. Electrostatic potential (ESP)-mapped van der Waals surfaces of A, LAS and SA molecules. ESP minima and maxima for different functional groups are shown as blue and yellow spheres, respectively, with their corresponding values (kcal mol^{-1}) indicated in parentheses. Red arrows denote preferred directions for hydrogen bond formation, while blue arrows illustrate likely pathways for proton transfer.

3.2.3 Atmospheric implications of LAS

In addition to temperature, the concentrations of precursors play a pivotal role in SA-A aerosol nucleation. Atmospheric LAS concentrations exhibit considerable variability across different global environments (Tan et al., 2022; Mochizuki et al., 2017; Ristovski et al., 2010; Hettiyadura et al., 2017; Kanellopoulos et al., 2022). For example, lower LAS concentrations, ranging from 1.00×10^4 to 8.34×10^5 molecules cm^{-3} , are found in regions such as eucalypt forest (Ristovski et al., 2010), Mt. Tai (China) (Mochizuki et al., 2017) and Athens (Kanellopoulos et al., 2022). In contrast, higher LAS concentrations have been recorded in Centreville, Alabama (1.77×10^6 molecules cm^{-3}) (Hettiyadura et al., 2017), with peak levels in Patra (Kanellopoulos et al., 2022), reaching up to 1.70×10^7 molecules cm^{-3} . Similarly, the concentrations of SA and A vary, with SA ranging from 10^4 – 10^7 molecules cm^{-3} (Zhang et al., 2024; Ding et al., 2019), and A ranging from 10^7 – 10^{11} molecules cm^{-3} (Wu et al., 2017; Luo et al., 2014). Elevated concentrations of these species are particularly prominent in regions such as northern China, the Midwestern United States, and agricultural areas in Europe. Based on field observations of LAS, SA and A concentrations, the contribution of LAS to SA-A nucleation was systematically assessed. As illustrated in Fig. S18, the impact of LAS on the SA-A system is primarily governed

by the concentrations of LAS and SA, with minimal dependence on [A]. Consequently, Fig. 6 illustrates how the contribution ratio of LAS varies with different concentrations of SA and LAS, under the previously identified favorable high-temperature condition of 278.15 K.

The three pie charts in the upper map illustrate the changing contribution of LAS to SA-A aerosol nucleation as SA concentration increases from 3.00×10^4 to 6.00×10^4 molecules cm^{-3} , with a corresponding decrease in LAS contribution as [SA] rises. In regions characterized by low SA concentrations (3.00×10^4 molecules cm^{-3}), such as Hyttiälä, nucleation is predominantly driven by the LAS-SA-A pathway, contributing approximately 93%. However, at higher SA concentrations (up to 2.00×10^6 molecules cm^{-3}), such as on the west coast of Ireland (O'Dowd et al., 2002), the LAS contribution drops from 93% to 33%. At even higher SA levels (up to 1.00×10^7 molecules cm^{-3}), LAS-involved pathways account for only 18% of the total nucleation flux, as observed in Beijing, China (Wang et al., 2011). In contrast, environments with typically high SA concentrations, such as urban and industrial areas, promote SA-A self-aggregation nucleation, thereby diminishing the relative contribution of LAS (Fig. S10). These findings highlight that lower [SA] levels substantially amplify the contribution of LAS contribution to SA-A aerosol nucleation.

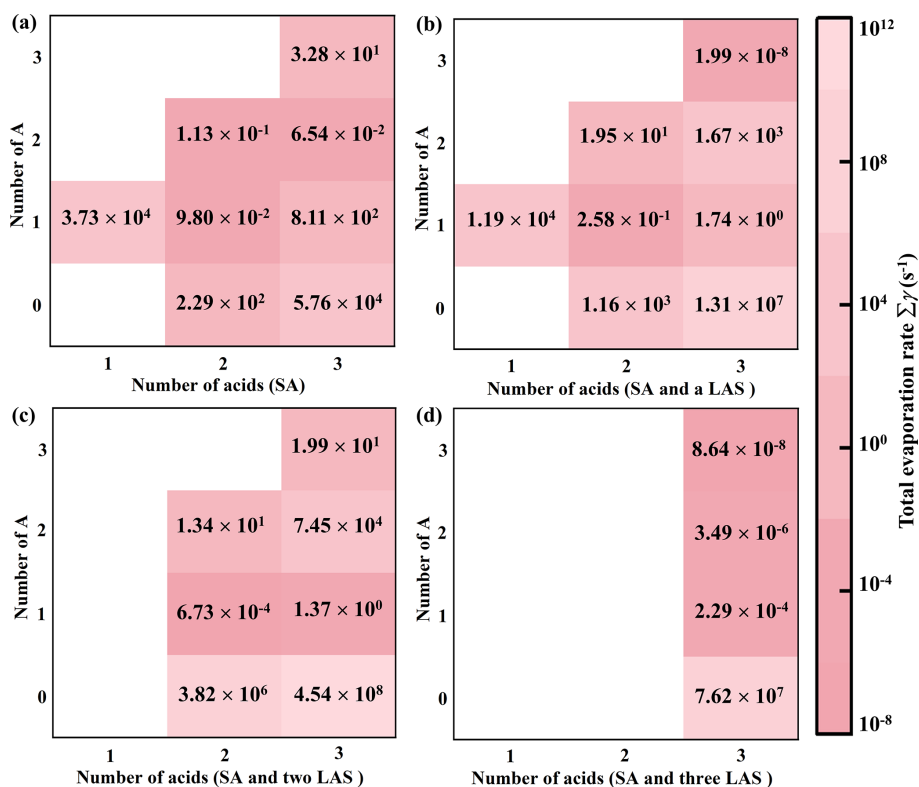


Figure 4. The total evaporation rates ($\sum \gamma$) (s^{-1}) of $(\text{SA})_x(\text{A})_y(\text{LAS})_z$ ($y \leq x + z \leq 3$) clusters at 278.15 K and 1 atm calculated at the M06-2X/6-311++G(2df, 2pd) level of theory. (a) without LAS monomer, (b) containing 1 LAS monomer, (c) containing 2 LAS monomers, and (d) containing 3 LAS monomers.

The contribution of LAS to SA-A aerosol nucleation increases with LAS concentration, ranging from 1.00×10^4 to 1.77×10^6 molecules cm^{-3} , as shown in the pie chart below the map. This pattern indicates a positive correlation between LAS concentration and its contribution to nucleation. In regions with low LAS concentrations (1.00×10^4 molecules cm^{-3}), such as eucalypt forests (Ristovski et al., 2010), LAS-mediated pathways account for only 15% of the total nucleation flux. While LAS contributes to the initial stages of cluster formation, it subsequently evaporates from the pre-nucleation cluster, ultimately functioning in a catalyst-like capacity (Fig. S16). In areas with moderate LAS concentrations, such as Athens (8.34×10^5 molecules cm^{-3}) (Kanellopoulos et al., 2022) and Mt. Tai (1.00×10^5 molecules cm^{-3}) (Mochizuki et al., 2017), LAS contribution increases substantially, rising from 15% to 73%. At high [LAS], as observed in the Centreville, Alabama (1.77×10^6 molecules cm^{-3}) (Hettiyadura et al., 2017), LAS-driven nucleation becomes dominant, resulting in a “participant” synergistic nucleation mechanism that works like “hand in hand” (Fig. S17), contributing up to 97% of the total nucleation rate. These findings underscore that elevated LAS concentrations significantly enhance SA-A nucleation. Thus, in regions characterized by high T , low [SA], high [A] and high [LAS], especially in agricultural-

developed areas and forested areas, the LAS contribution to SA-A aerosol nucleation can be substantial.

3.3 The comparison of enhancement effect between LAS and LA

To evaluate the relative enhancing effects of LA versus LAS in the typical SA-A-driven nucleation. The ΔG (pink histograms) and $\sum \gamma$ (red points) of the $(\text{LAS})_x(\text{SA})_y(\text{A})_3$ and $(\text{LA})_x(\text{SA})_y(\text{A})_3$ ($x = 0-3$, $x + y = 3$) clusters at 278.15 K are presented in Fig. 7a as a comparison. The $(\text{SA})_3(\text{A})_3$ cluster, the thermodynamic minimum of the SA-A system (Chen et al., 2025; Li et al., 2020), was chosen as a reference for comparison. Relative to this baseline, $(\text{LA})_{1-3}(\text{SA})_{0-2}(\text{A})_3$ clusters consistently exhibited higher ΔG values, elevated by roughly 18.36–41.94 kcal mol^{-1} . In contrast, $(\text{LAS})_{1-3}(\text{SA})_{0-2}(\text{A})_3$ clusters were slightly more stable, differing from the reference by only 0.09–5.80 kcal mol^{-1} . This suggests that LAS incorporation leads to a slight stabilization of the cluster relative to LA.

Moreover, the evaporation rate ($\sum \gamma$) of the $(\text{Org})_x(\text{SA})_y(\text{A})_3$ (Org = LA and LAS; $x = 1-3$, $x + y = 3$) clusters do not exhibit a simple relationship with the proportion of organic components within the clusters. The highest $\sum \gamma$ was observed for the $(\text{Org})_2 \cdot (\text{SA})_1 \cdot (\text{A})_3$ (Org = LA

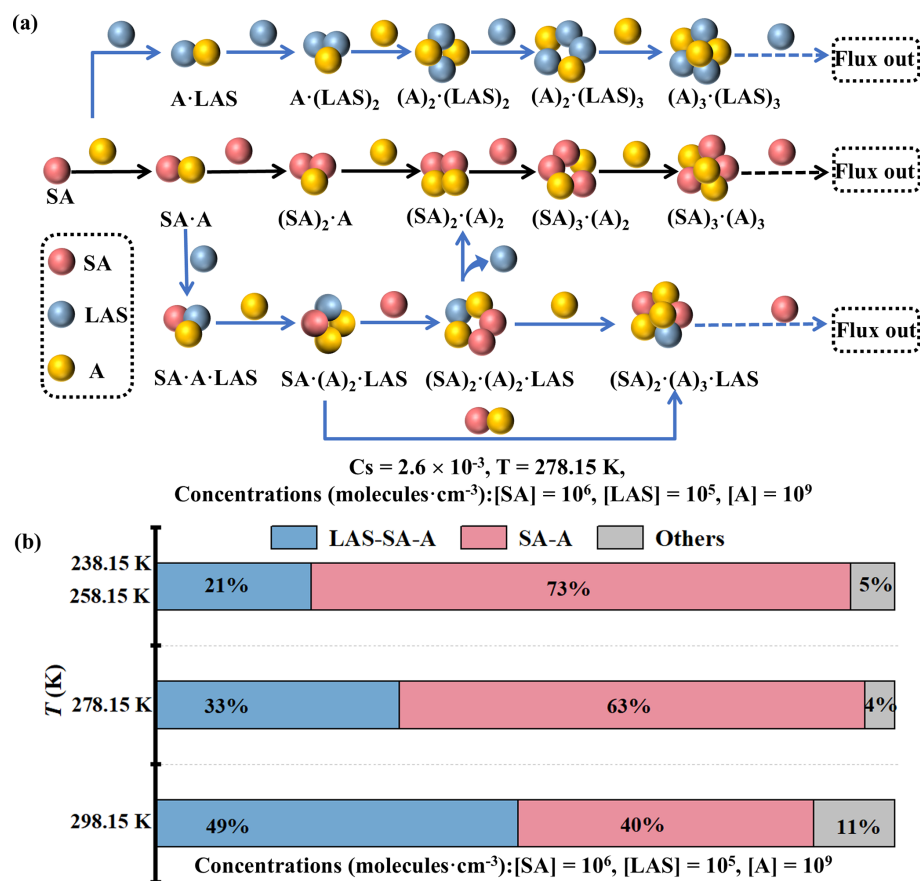


Figure 5. Nucleation mechanism of the LAS-SA-A system. (a) Cluster formation pathway at 278.15 K, with concentrations of [SA] = 10^6 , [A] = 10^9 and [LAS] = 10^5 molecules cm^{-3} ; (b) the branch ratio of outward flux at different temperatures. Only net fluxes contributing more than 5 % to cluster growth are depicted.

and LAS) clusters, regardless of whether LA or LAS was used. For the $(LAS)_1 \cdot (SA)_2 \cdot (A)_3$ and $(LAS)_3 \cdot (A)_3$ clusters, the $\sum \gamma$ ranged from 10^{-4} to 10^{-1} s^{-1} , lower than that of the $(SA)_3 \cdot (A)_3$ cluster, indicating that replacing one or three SA molecules with LAS enhances the thermodynamic stability of the clusters. In contrast, the $\sum \gamma$ of the LA-SA-A clusters were found to be higher than those of the corresponding LAS-SA-A and $(SA)_3 \cdot (A)_3$ clusters, as displayed in Fig. 7a. The LAS-SA-A clusters exhibit more negative ΔG values and lower $\sum \gamma$, suggesting that their formation is thermodynamically more favorable than that of the LA-SA-A system. This enhanced stability can be attributed to stronger interactions between LAS and SA-A systems relative to those between LA and SA-A. Based on these results, we can conclude that LAS, produced through the LA + SO $_3$ reaction, more effectively stabilizes the SA-A system than LA itself.

Figure 7b illustrates the variation in the cluster formation rate (J) and enhancement strength (R) as a function of [LAS] and [LA] at 278.15 K, under the condition of [SA] = 10^6 molecules cm^{-3} and [A] = 10^9 molecules cm^{-3} . In the LAS-SA-A system, J

increases sharply with rising [LAS], particularly when [LAS] exceeds 10^5 molecules cm^{-3} . As [LAS] grows from 10^5 to 10^6 molecules cm^{-3} , J for the LAS-SA-A system rises by three orders of magnitude, whereas in the LA-SA-A system, J exhibits only a modest increase from 3.36×10^{-9} to $1.12 \times 10^{-8} \text{ cm}^{-3} \text{ s}^{-1}$, consistent with the corresponding increase in [LA] (Fig. 7b). Although LAS concentrations are typically three orders of magnitude lower than LA (Tan et al., 2022), LAS exerts a substantially stronger enhancement effect in SA-A-driven nucleation. These contrasting trends are primarily due to the combined influence of cluster thermodynamic properties ΔG and $\sum \gamma$, and the concentrations of organic species within the respective systems. The sharp increase in J for the LAS-SA-A system stems from the favorable ΔG and low $\sum \gamma$ of the $(LAS)_x(SA)_y(A)_z$ clusters, along with the relatively high non-equilibrium concentration of LAS. In contrast, the less favorable ΔG and higher $\sum \gamma$ of the $(LA)_x(SA)_y(A)_z$ clusters limit the kinetic efficiency of the LA-SA-A system, even at elevated [LA].

This study reveals that the reaction of LA and SO $_3$ generates LAS which acts as an effective atmospheric nucleation precursor and significantly accelerates SA-A nucle-

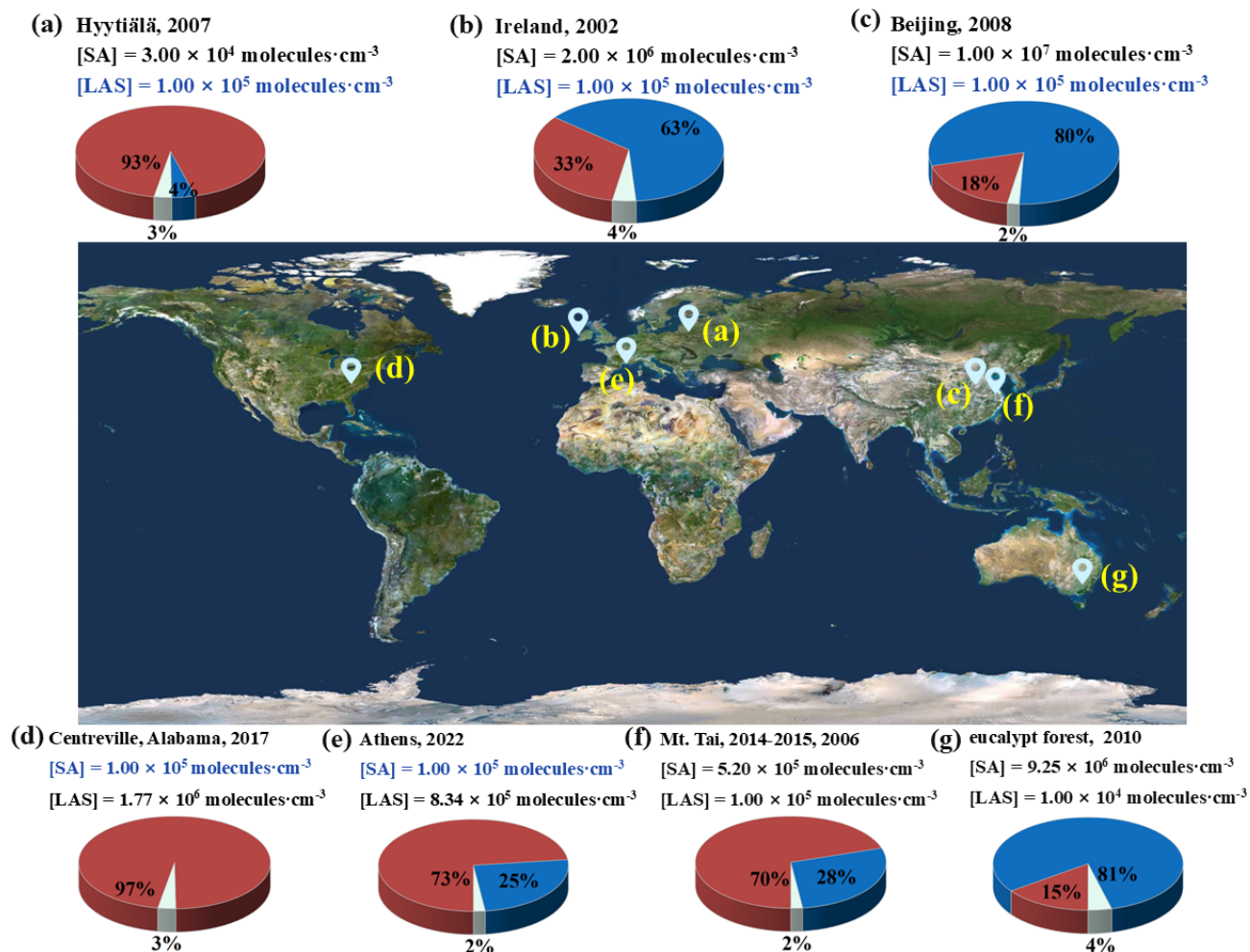


Figure 6. Branching ratios of SA-A-LAS (red) and SA-A (blue) cluster growth pathways in regions with varying [LAS] concentrations. Black data points indicate field observations, while blue points represent the median values used in this study. Ammonia concentration is fixed at 10^9 molecules cm⁻³. Imagery © 2024 Google, Map data © 2024 Google.

ation. Consequently, atmospheric LA can react with part of SO₃, potentially accounting for the relatively low observed low SA concentration, while the generated LAS markedly promotes SA-A-driven NPF under such conditions. To date, the effects of hydroxy acids and their derivatives on atmospheric NPF have not been comprehensively investigated. The mechanism proposed here offers a general approach to evaluate the roles of these acids, like 2-Methylglyceric acid, aromatic acids and their derivatives, influence atmospheric nucleation processes. Incorporating this novel OS pathways into contemporary atmospheric models will advance the quantitative understanding of OS' contributions to aerosol formation. Furthermore, OS originating from secondary processes, such as gas-phase chemical reactions, deserve further observation and evaluation.

4 Conclusions

In this study, quantum chemical calculations, master equation analysis, and the ACDC kinetic model were employed to investigate the cycloaddition reaction between SO₃ and LA, the role of LAS in SA-A nucleation, and its impact on NPF.

Quantum chemical results in the gas phase indicate that SA and H₂O effectively lower the reaction barriers for LAS formation from the LA-SO₃ reaction, functioning as catalysts and even enabling a barrierless reaction. The effective rate coefficient for the SO₃-LA reaction catalyzed by SA (10^7 molecules cm⁻³) is 4–5 times higher than the pathway catalyzed by H₂O (10^{17} molecules cm⁻³), making it more effective, particularly at altitudes of 5–10 km. Additionally, the effective rate coefficients for LA (10^{12} molecules cm⁻³) catalyzing the SO₃+H₂O → SA reaction is about 10^1 – 10^4 times larger than the corresponding values for SO₃ hy-

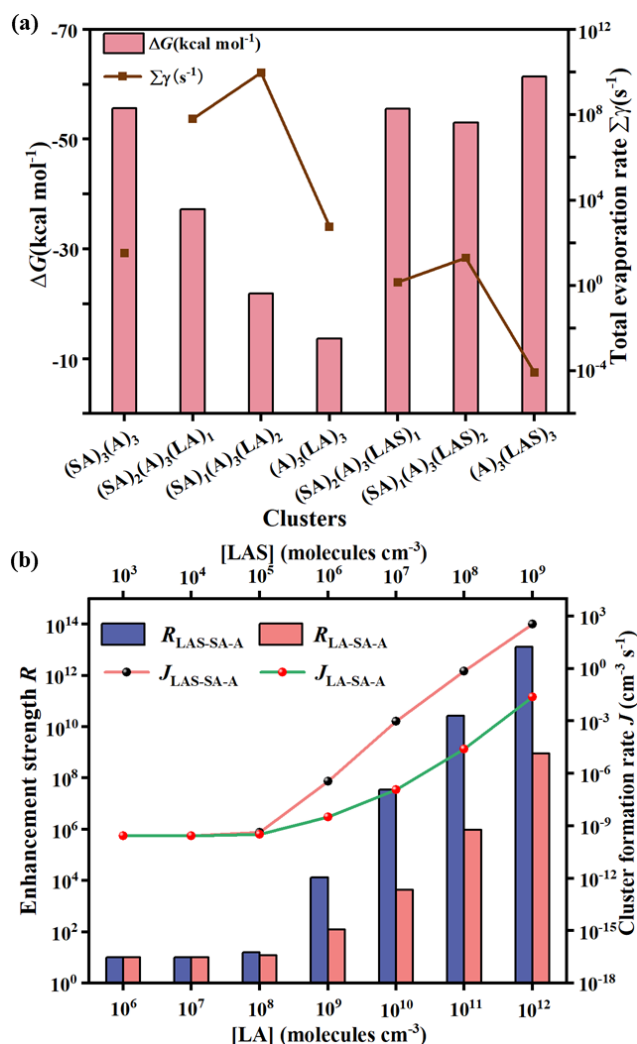


Figure 7. (a) Gibbs free energies ΔG (kcal mol⁻¹) and total evaporation rates $\sum \gamma$ (s⁻¹) for (LA)_x(SA)_y(A)₃ and (LAS)_x(SA)_y(A)₃ ($x = 0-3$, $x + y = 3$) clusters calculated at the M06-2X/6-311++G(2df, 2pd) level of theory and 278.15 K; (b) Cluster formation rate (J) and enhancement strength (R) for LAS as a function of monomer concentrations ([LA] and [LAS]) at 278.15 K, with [SA] fixed at 10⁵ molecules cm⁻³ and [A] at 10⁹ molecules cm⁻³.

drolisis catalyzed by H₂SO₄ (10⁷ molecules cm⁻³), HNO₃ (10⁹ molecules cm⁻³), HCOOH (10¹¹ molecules cm⁻³), and OA (10⁹ molecules cm⁻³), indicating that LA primarily catalyzes SO₃ hydrolysis within the temperature range of 280–320 K.

LAS, functioning as both a hydrogen-bond donor and acceptor, participates in SA-A-driven ternary nucleation, directly interacting with SA and A. Gibbs free energy analysis demonstrates that ternary SA-A-LAS clusters consistently exhibit lower ΔG values than their binary counterparts, suggesting that LAS incorporation stabilizes the SA-A clusters. ACDC kinetic simulations further demonstrate that LAS significantly enhances NPF, especially at low temperatures, low

SA concentration, and high A and LAS concentrations. In regions with elevated LAS concentrations, such as Centreville, Alabama, particle formation rates can increase by up to 10⁸-fold, with SA-A-LAS clusters contributing up to 97 % of the overall cluster formation pathways. It is noteworthy that LAS not only acts as a catalyst in enhancing SA-A cluster stability but also directly participates in nucleation. Moreover, LAS exerts a stronger enhancement effect than LA, making it a more effective stabilizing agent for atmospheric NPF. These findings suggest that LAS plays a critical role in enhancing SA-A-driven NPF in forested and agriculturally developed regions, providing insights into previously unaccounted NPF sources and refining nucleation models.

This study deepens the understanding of OSs formation in organic acid-polluted regions and underscores the potential contribution of other OSs to NPF. Neglecting the contribution of OSs in the SA-A aerosol nucleation, particularly in forested and agricultural regions, may lead to an underestimation of organic aerosol nucleation risks.

Data availability. Data will be made available on request.

Supplement. The supplement related to this article is available online at <https://doi.org/10.5194/acp-26-3091-2026-supplement>.

Author contributions. RW: writing (original draft) and funding acquisition; SW: methodology, investigation, data curation, visualization, data computation and writing (original draft); ZL: data curation, methodology and investigation; KX: data curation, visualization and investigation; RB: data curation and project administration; TZ: writing (review and editing) and funding acquisition. All the authors contributed to revise the manuscript and approve the final version.

Competing interests. The contact author has declared that none of the authors has any competing interests.

Disclaimer. Publisher's note: Copernicus Publications remains neutral with regard to jurisdictional claims made in the text, published maps, institutional affiliations, or any other geographical representation in this paper. The authors bear the ultimate responsibility for providing appropriate place names. Views expressed in the text are those of the authors and do not necessarily reflect the views of the publisher.

Acknowledgements. This work was supported by the National Natural Science Foundation of China (grant nos. 22203052 and 22073059) and the Funds of Graduate Innovation of Shaanxi University of Technology (grant no. SLGYCX2506).

Financial support. This research has been supported by the Foundation for Innovative Research Groups of the National Natural Science Foundation of China (grant nos. 22203052 and 22073059) and the Funds of Graduate Innovation of Shaanxi University of Technology (grant no. SLGYCX2506).

Review statement. This paper was edited by Manabu Shiraiwa and reviewed by three anonymous referees.

References

- Anderson, J. O., Thundiyil, J. G., and Stolbach, A.: Clearing the air: a review of the effects of particulate matter air pollution on human health, *J. Med. Toxicol.*, 8, 166–175, 2012.
- Brean, J., Beddows, D. C. S., Shi, Z., Temime-Roussel, B., Marchand, N., Querol, X., Alastuey, A., Minguillón, M. C., and Harrison, R. M.: Molecular insights into new particle formation in Barcelona, Spain, *Atmos. Chem. Phys.*, 20, 10029–10045, <https://doi.org/10.5194/acp-20-10029-2020>, 2020.
- Brüggemann, M., Poulain, L., Held, A., Stelzer, T., Zuth, C., Richters, S., Mutzel, A., van Pinxteren, D., Iinuma, Y., Katkevica, S., Rabe, R., Herrmann, H., and Hoffmann, T.: Real-time detection of highly oxidized organosulfates and BSOA marker compounds during the F-BEACH 2014 field study, *Atmos. Chem. Phys.*, 17, 1453–1469, <https://doi.org/10.5194/acp-17-1453-2017>, 2017.
- Cai, R., Yan, C., Yang, D., Yin, R., Lu, Y., Deng, C., Fu, Y., Ruan, J., Li, X., Kontkanen, J., Zhang, Q., Kangasluoma, J., Ma, Y., Hao, J., Worsnop, D. R., Bianchi, F., Paasonen, P., Kerminen, V.-M., Liu, Y., Wang, L., Zheng, J., Kulmala, M., and Jiang, J.: Sulfuric acid–amine nucleation in urban Beijing, *Atmos. Chem. Phys.*, 21, 2457–2468, <https://doi.org/10.5194/acp-21-2457-2021>, 2021.
- Chen, S. S., Li, R. R., Zhang, C. Y., Wei, S. Q., Wang, R., Chu, B. W., Zhang, X. M., Li, H., and Zhang, T. L.: The enhanced role of formic acid on sulfuric acid–ammonia–driven nucleation in forest regions and polluted city areas, *J. Environ. Sci.*, 160, 621–628, 2025.
- Cheng, Y., Wang, R., Chen, Y., Tian, S., Gao, N., Zhang, Z., and Zhang, T.: Hydrolysis of SO₃ in small clusters of sulfuric acid: mechanistic and kinetic study, *ACS Earth and Space Chemistry*, 6, 3078–3089, 2022.
- Dai, L., Zhao, Y., Zhang, L., Chen, D., and Wu, R.: Particle number size distributions and formation and growth rates of different new particle formation types of a megacity in China, *J. Environ. Sci.*, 131, 11–25, 2023.
- Darer, A. I., Cole-Filipiak, N. C., O'Connor, A. E., and Elrod, M. J.: Formation and stability of atmospherically relevant isoprene-derived organosulfates and organonitrates, *Environ. Sci. Technol.*, 45, 1895–1902, 2011.
- Ding, J., Zhao, P., Su, J., Dong, Q., Du, X., and Zhang, Y.: Aerosol pH and its driving factors in Beijing, *Atmos. Chem. Phys.*, 19, 7939–7954, <https://doi.org/10.5194/acp-19-7939-2019>, 2019.
- Faloon, I., Conley, S. A., Blomquist, B., Clarke, A. D., Kapustin, V., Howell, S., Lenschow, D. H., and Bandy, A. R.: Sulfur dioxide in the tropical marine boundary layer: dry deposition and heterogeneous oxidation observed during the pacific atmospheric sulfur experiment, *J. Atmos. Chem.*, 63, 13–32, 2009.
- Froyd, K. D., Murphy, S. M., Murphy, D. M., de Gouw, J. A., Edgingaas, N. C., and Wennberg, P. O.: Contribution of isoprene-derived organosulfates to free tropospheric aerosol mass, *P. Natl. Acad. Sci. USA*, 107, 21360–21365, 2010a.
- Glasius, M., Hansen, A. M. K., Claeys, M., Henzing, B., Jedyńska, A., Kasper-Giebl, A., Kistler, M., Kristensen, K., Martinsson, J., Maenhaut, W., Nøjgaard, J., Spindler, G., Stenström, K., Swietlicki, E., Szidat, S., Simpson, D., and Yttri, K. E.: Composition and sources of carbonaceous aerosols in Northern Europe during winter, *Atmos. Environ.*, 173, 127–141, 2017.
- Glowacki, D. R., Liang, C. H., Morley, C., Pilling, M. J., and Robertson, S. H.: MESMER: an open-source master equation solver for multi-energy well reactions, *J. Phys. Chem. A*, 116, 9545–9560, 2012.
- Hazra, M. K. and Sinha, A.: Formic acid catalyzed hydrolysis of SO₃ in the gas phase: a barrierless mechanism for sulfuric acid production of potential atmospheric importance, *J. Am. Chem. Soc.*, 133, 17444–17453, 2011.
- Hettiyadura, A. P. S., Jayarathne, T., Baumann, K., Goldstein, A. H., de Gouw, J. A., Koss, A., Keutsch, F. N., Skog, K., and Stone, E. A.: Qualitative and quantitative analysis of atmospheric organosulfates in Centreville, Alabama, *Atmos. Chem. Phys.*, 17, 1343–1359, <https://doi.org/10.5194/acp-17-1343-2017>, 2017.
- Hirsikko, A., Nieminen, T., Gagné, S., Lehtipalo, K., Manninen, H. E., Ehn, M., Hörrak, U., Kerminen, V.-M., Laakso, L., McMurry, P. H., Mirme, A., Mirme, S., Petäjä, T., Tammets, H., Vakkari, V., Vana, M., and Kulmala, M.: Atmospheric ions and nucleation: a review of observations, *Atmos. Chem. Phys.*, 11, 767–798, <https://doi.org/10.5194/acp-11-767-2011>, 2011.
- Hodshire, A. L., Campuzano-Jost, P., Kodros, J. K., Croft, B., Nault, B. A., Schroder, J. C., Jimenez, J. L., and Pierce, J. R.: The potential role of methanesulfonic acid (MSA) in aerosol formation and growth and the associated radiative forcings, *Atmos. Chem. Phys.*, 19, 3137–3160, <https://doi.org/10.5194/acp-19-3137-2019>, 2019.
- Horváth, G., Horváth, I., Almousa, S. A. D., and Telek, M.: Numerical inverse laplace transformation using concentrated matrix exponential distributions, *Performance Evaluation*, 137, 102067, <https://doi.org/10.1016/j.peva.2019.102067>, 2020.
- Hratchian, H. P. and Schlegel, H. B.: Using hessian updating to increase the efficiency of a hessian based predictor–corrector reaction path following method, *J. Chem. Theory Comput.* 1, 61–69, 2005.
- Huang, H. L., Chao, W., and Lin, J. J. M.: Kinetics of a Criegee intermediate that would survive high humidity and may oxidize atmospheric SO₂, *P. Natl. Acad. Sci. USA*, 112, 10857–10862, 2015.
- Kanellopoulos, P. G., Kotsaki, S. P., Chrysochou, E., Koukoulakis, K., Zacharopoulos, N., Philippopoulos, A., and Bakeas, E.: PM_{2.5}-bound organosulfates in two Eastern Mediterranean cities: The dominance of isoprene organosulfates, *Chemosphere*, 297, 134103, <https://doi.org/10.1016/j.chemosphere.2022.134103>, 2022.
- Kirkby, J., Curtius, J., Almeida, J., Dunne, E., Duplissy, J., Ehrhart, S., Franchin, A., Gagné, S., Ickes, L., Kürten, A., Kupc, A., Metzger, A., Riccobono, F., Rondo, L., Schobesberger, S., Tsagkogeorgas, G., Wimmer, D., Amorim, A., Bianchi, F., Breitenlechner,

- M., David, A., Dommen, J., Downard, A., Ehn, M., Flagan, R. C., Haider, S., Hansel, A., Hauser, D., Jud, W., Junninen, H., Kreissl, F., Kvashin, A., Laaksonen, A., Lehtipalo, K., Lima, J., Lovejoy, E. R., Makhmutov, V., Mathot, S., Mikkilä, J., Minginette, P., Mogo, S., Nieminen, T., Onnela, A., Pereira, P., Petäjä, T., Schnitzhofer, R., Seinfeld, J. H., Sipilä, M., Stozhkov, Y., Stratmann, F., Tomé, A., Vanhanen, J., Viisanen, Y., Vrtala, A., Wagner, P. E., Walther, H., Weingartner, E., Wex, H., Winkler, P. M., Carslaw, K. S., Worsnop, D. R., Baltensperger, U., and Kulmala, M.: Role of sulphuric acid, ammonia and galactic cosmic rays in atmospheric aerosol nucleation, *Nature*, 476, 429–433, 2011.
- Kirkby, J., Duplissy, J., Sengupta, K., Frege, C., Gordon, H., Williamson, C., Heinritzi, M., Simon, M., Yan, C., Almeida, J., Tröstl, J., Nieminen, T., Ortega, I. K., Wagner, R., Adamov, A., Amorim, A., Bernhammer, A.-K., Bianchi, F., Breitenlechner, M., Brilke, S., Chen, X., Craven, J., Dias, A., Ehrhart, S., Flagan, R. C., Franchin, A., Fuchs, C., Guida, R., Hakala, J., Hoyle, C. R., Jokinen, T., Junninen, H., Kangasluoma, J., Kim, J., Krapf, M., Kürten, A., Laaksonen, A., Lehtipalo, K., Makhmutov, V., Mathot, S., Molteni, U., Onnela, A., Peräkylä, O., Piel, F., Petäjä, T., Praplan, A. P., Pringle, K., Rap, A., Richards, N. A. D., Riipinen, I., Rissanen, M. P., Rondo, L., Sarnela, N., Schobesberger, S., Scott, C. E., Seinfeld, J. H., Sipilä, M., Steiner, G., Stozhkov, Y., Stratmann, F., Tomé, A., Virtanen, A., Vogel, A. L., Wagner, A. C., Wagner, P. E., Weingartner, E., Wimmer, D., Winkler, P. M., Ye, P., Zhang, X., Hansel, A., Dommen, J., Donahue, N. M., Worsnop, D. R., Baltensperger, U., Kulmala, M., Carslaw, K. S., and Curtius, J.: Ion-induced nucleation of pure biogenic particles, *Nature*, 533, 521–526, 2016.
- Klippenstein, S. J. and Marcus, R. A.: Unimolecular reaction rate theory for highly flexible transition states. 2. Conventional coordinate formulas for the various possible fragment combinations: miscellaneous topics, *J. Phys. Chem. C.*, 92, 5412–5417, 1988.
- Kulmala, M., Vehkamäki, H., Petäjä, T., Dal Maso, M., Lauri, A., Kerminen, V. M., Birmili, W., and McMurry, P. H.: Formation and growth rates of ultrafine atmospheric particles: a review of observations, *Aerosol Sci.*, 35, 143–176, 2004.
- Kundu, S., Quraishi, T. A., Yu, G., Suarez, C., Keutsch, F. N., and Stone, E. A.: Evidence and quantitation of aromatic organosulfates in ambient aerosols in Lahore, Pakistan, *Atmos. Chem. Phys.*, 13, 4865–4875, <https://doi.org/10.5194/acp-13-4865-2013>, 2013.
- Kurtén, T., Loukonen, V., Vehkamäki, H., and Kulmala, M.: Amines are likely to enhance neutral and ion-induced sulfuric acid-water nucleation in the atmosphere more effectively than ammonia, *Atmos. Chem. Phys.*, 8, 4095–4103, <https://doi.org/10.5194/acp-8-4095-2008>, 2008.
- Lee, S. H., Gordon, H., Yu, H., Lehtipalo, K., Haley, R., Li, Y., and Zhang, R.: New particle formation in the atmosphere: from molecular clusters to global climate, *J. Geophys. Res.-Atmos.*, 124, 7098–7146, 2019.
- Li, D., Chen, D., Liu, F., and Wang, W.: Role of glycine on sulfuric acid-ammonia clusters formation: Transporter or participator, *J. Environ. Sci.*, 89, 125–135, 2020.
- Li, H., Kupiainen-Määttä, O., Zhang, H., Zhang, X., and Ge, M.: A molecular-scale study on the role of lactic acid in new particle formation: Influence of relative humidity and temperature, *Atmos. Environ.*, 166, 479–487, 2017.
- Li, H., Zhong, J., Vehkamäki, H., Kurtén, T., Wang, W., Ge, M., Zhang, S., Li, Z., Zhang, X., Francisco, J. S., and Zeng, X. C.: Self-catalytic reaction of SO₃ and NH₃ to produce sulfamic acid and its implication to atmospheric particle formation, *J. Am. Chem. Soc.*, 140, 11020–11028, 2018a.
- Li, J., Tsona, N. T., and Du, L.: Effect of a single water molecule on the HO₂+ ClO reaction, *Phys. Chem. Chem. Phys.*, 20, 10650–10659, 2018b.
- Li, J., Ning, A., Liu, L., and Zhang, X.: Atmospheric bases enhanced iodine acid nucleation: altitude-dependent characteristics and molecular mechanisms, *Environ. Sci. Technol.*, 58, 16962–16973, 2024.
- Liu, L., Zhong, J., Vehkamäki, H., Kurtén, T., Du, L., Zhang, X., Francisco, J. S., and Zeng, X. C.: Unexpected quenching effect on new particle formation from the atmospheric reaction of methanol with SO₃, *P. Natl. Acad. Sci. USA*, 116, 24966–24971, 2019.
- Liu, L., Yu, F., Du, L., Yang, Z., Francisco, J. S., and Zhang, X.: Rapid sulfuric acid-dimethylamine nucleation enhanced by nitric acid in polluted regions, *P. Natl. Acad. Sci. USA*, 118, e2108384118, <https://doi.org/10.1073/pnas.2108384118>, 2021.
- Long, B., Chang, C. R., Long, Z. W., Wang, Y. B., Tan, X. F., and Zhang, W. J.: Nitric acid catalyzed hydrolysis of SO₃ in the formation of sulfuric acid: a theoretical study, *Chem. Phys. Lett.*, 581, 26–29, 2013.
- Lu, T. and Chen, F.: Multiwfn: a multifunctional wavefunction analyzer, *J. Comput. Chem.*, 33, 580–592, 2012.
- Lu, Y., Liu, L., Ning, A., Gan, Y., Liu, Y., Kurtén, T., Vehkamäki, H., and Wang, L.: Atmospheric sulfuric acid-dimethylamine nucleation enhanced by trifluoroacetic acid, *Geophys. Res. Lett.*, 47, <https://doi.org/10.1029/2019GL085627>, 2020.
- Lund, M. T., Myhre, G., and Samset, B. H.: Anthropogenic aerosol forcing under the Shared Socioeconomic Pathways, *Atmos. Chem. Phys.*, 19, 13827–13839, <https://doi.org/10.5194/acp-19-13827-2019>, 2019.
- Luo, X. S., Tang, A. H., Shi, K., Wu, L. H., Li, W. Q., Shi, W. Q., Shi, X. K., Erisman, J. W., Zhang, F. S., and Liu, X. J.: Chinese coastal seas are facing heavy atmospheric nitrogen deposition, *Environ. Res. Lett.*, 9, <https://doi.org/10.1088/1748-9326/9/9/095007>, 2014.
- Lv, G., Sun, X., Zhang, C., and Li, M.: Understanding the catalytic role of oxalic acid in SO₃ hydration to form H₂SO₄ in the atmosphere, *Atmos. Chem. Phys.*, 19, 2833–2844, <https://doi.org/10.5194/acp-19-2833-2019>, 2019.
- Ma, F., Xie, H. B., Elm, J., Shen, J., Chen, J., and Vehkamäki, H.: Piperazine enhancing sulfuric acid-based new particle formation: implications for the atmospheric fate of piperazine, *Environ. Sci. Technol.*, 53, 8785–8795, 2019.
- Mai, T. V., Duong, M. V., Nguyen, H. T., and Huynh, L. K.: Ab initio kinetics of the HOSO₂+³O₂ → SO₃+ HO₂ reaction, *Phys. Chem. Chem. Phys.*, 20, 6677–6687, 2018.
- Mochizuki, T., Kawamura, K., Nakamura, S., Kanaya, Y., and Wang, Z.: Enhanced levels of atmospheric low-molecular weight monocarboxylic acids in gas and particulates over Mt. Tai, North China, during field burning of agricultural wastes, *Atmos. Environ.*, 171, 237–247, 2017.
- Mochizuki, T., Kawamura, K., Miyazaki, Y., Kunwar, B., and Boreddy, S. K. R.: Distributions and sources of low-molecular-weight monocarboxylic acids in gas and particles from a decidu-

- ous broadleaf forest in northern Japan, *Atmos. Chem. Phys.*, 19, 2421–2432, <https://doi.org/10.5194/acp-19-2421-2019>, 2019.
- Mutzel, A., Poulain, L., Berndt, T., Iinuma, Y., Rodigast, M., Böge, O., Richters, S., Spindler, G., Sipilä, M., Jokinen, T., Kulmala, M., and Herrmann, H.: Highly oxidized multifunctional organic compounds observed in tropospheric particles: a field and laboratory study, *Environ. Sci. Technol.*, 49, 7754–7761, 2015.
- Neese, F.: The ORCA program system, *WIREs Computational Molecular Science*, 2, 73–78, 2012.
- O'Dowd, C. D., Hämeri, K., Mäkelä, J. M., Pirjola, L., Kulmala, M., Jennings, S. G., Berresheim, H., Hansson, H. C., de Leeuw, G., Kunz, G. J., Allen, A. G., Hewitt, C. N., Jackson, A., Viisanen, Y., and Hoffmann, T.: A dedicated study of New Particle Formation and Fate in the Coastal Environment (PARFORCE): Overview of objectives and achievements, *J. Geophys. Res.-Atmos.*, 107, <https://doi.org/10.1029/2001JD000555>, 2002.
- Olson, C. N., Galloway, M. M., Yu, G., Hedman, C. J., Lockett, M. R., Yoon, T., Stone, E. A., Smith, L. M., and Keutsch, F. N.: Hydroxycarboxylic acid-derived organosulfates: synthesis, stability, and quantification in ambient aerosol, *Environ. Sci. Technol.*, 45, 6468–6474, 2011.
- Partanen, L., Vehkamäki, H., Hansen, K., Elm, J., Henschel, H., Kurtén, T., Halonen, R., and Zapadinsky, E.: Effect of conformers on free energies of atmospheric complexes, *J. Phys. Chem. A*, 120, 8613–8624, 2016.
- Ristovski, Z. D., Suni, T., Kulmala, M., Boy, M., Meyer, N. K., Duplissy, J., Turnipseed, A., Morawska, L., and Baltensperger, U.: The role of sulphates and organic vapours in growth of newly formed particles in a eucalypt forest, *Atmos. Chem. Phys.*, 10, 2919–2926, <https://doi.org/10.5194/acp-10-2919-2010>, 2010.
- Riva, M., Tomaz, S., Cui, T., Lin, Y.-H., Perraudin, E., Gold, A., Stone, E. A., Villenave, E., and Surratt, J. D.: Evidence for an unrecognized secondary anthropogenic source of organosulfates and sulfonates: gas-phase oxidation of polycyclic aromatic hydrocarbons in the presence of sulfate aerosol, *Environ. Sci. Technol.*, 49, 6654–6664, 2015.
- Rong, H., Liu, J. R., Zhang, Y. J., Du, L., Zhang, X., and Li, Z.: Nucleation mechanisms of iodic acid in clean and polluted coastal regions, *Chemosphere*, 253, 126743–126752, 2020a.
- Rong, H., Liu, L., Liu, J., and Zhang, X.: Glyoxylic sulfuric anhydride from the gas-phase reaction between Glyoxylic Acid and SO₃: A potential nucleation precursor, *J. Phys. Chem. A*, 124, 3261–3268, 2020b.
- Shampine, L. F. and Reichelt, M. W.: The MATLAB ode suite, *SIAM Journal on Scientific Computing*, 18, 1–22, 1997.
- Shen, J., Xie, H.-B., Elm, J., Ma, F., Chen, J., and Vehkamäki, H.: Methanesulfonic Acid-driven new particle formation enhanced by monoethanolamine: A computational study, *Environ. Sci. Technol.*, 53, 14387–14397, 2019.
- Shen, J., Elm, J., Xie, H. B., Chen, J., Niu, J., and Vehkamäki, H.: Structural effects of amines in enhancing methanesulfonic acid-driven new particle formation, *Environ. Sci. Technol.*, 54, 13498–13508, 2020.
- Sipilä, M., Sarnela, N., Jokinen, T., Henschel, H., Junninen, H., Kontkanen, J., Richters, S., Kangasluoma, J., Franchin, A., Peräkylä, O., Rissanen, M. P., Ehn, M., Vehkamäki, H., Kurten, T., Berndt, T., Petäjä, T., Worsnop, D., Ceburnis, D., Kerminen, V.-M., Kulmala, M., and O'Dowd, C.: Molecular-scale evidence of aerosol particle formation via sequential addition of HIO₃, *Nature*, 537, 532–534, 2016.
- Smith, C. J., Huff, A. K., Ward, R. M., and Leopold, K. R.: Carboxylic sulfuric anhydrides, *J. Phys. Chem. A*, 124, 601–612, 2020.
- Stewart, J. J.: Optimization of parameters for semiempirical methods V: modification of NDDO approximations and application to 70 elements, *J. Mol. Model.*, 13, 1173–1213, 2007.
- Sun, H., Liu, Y., Nie, W., Li, Y., Ge, D., Xu, T., Yin, J., Liu, C., Fu, Z., Qi, X., Liu, T., Zha, Q., Yan, C., Wang, Z., Chi, X., and Ding, A.: Unexpected gas-Phase formation of Glycolic Acid Sulfate in the atmosphere, *Environ. Sci. Technol.*, 59, 16556–16566, 2025.
- Tan, S., Zhang, X., Lian, Y., Chen, X., Yin, S., Du, L., and Ge, M.: OH group orientation leads to organosulfate formation at the liquid aerosol surface, *J. Am. Chem. Soc.*, 144, 16953–16964, 2022.
- Tan, X. F., Long, B., Ren, D. S., Zhang, W. J., Long, Z. W., and Mitchell, E.: Atmospheric chemistry of CH₃CHO: the hydrolysis of CH₃CHO catalyzed by H₂SO₄, *Phys. Chem. Chem. Phys.*, 20, 7701–7709, 2018.
- Tan, X. F., Zhang, L., and Long, B.: New mechanistic pathways for the formation of organosulfates catalyzed by ammonia and carbinolamine formation catalyzed by sulfuric acid in the atmosphere, *Phys. Chem. Chem. Phys.*, 22, 8800–8807, 2020.
- Tsona Tchinda, N., Du, L., Liu, L., and Zhang, X.: Pyruvic acid, an efficient catalyst in SO₃ hydrolysis and effective clustering agent in sulfuric-acid-based new particle formation, *Atmos. Chem. Phys.*, 22, 1951–1963, <https://doi.org/10.5194/acp-22-1951-2022>, 2022.
- Walker, M., Harvey, A. J. A., Sen, A., and Dessent, C. E. H.: Performance of M06, M06-2X, and M06-HF density functionals for conformationally flexible anionic clusters: M06 functionals perform better than B3LYP for a model system with dispersion and ionic hydrogen-bonding interactions, *J. Phys. Chem. A*, 117, 12590–12600, 2013.
- Wang, R., Li, R., Chen, S., Mu, R., Zhang, C., Ma, X., Khan, M., and Zhang, T.: Enhancing SO₃ hydrolysis and nucleation: the role of formic sulfuric anhydride, *Atmos. Chem. Phys.*, 25, 5695–5709, <https://doi.org/10.5194/acp-25-5695-2025>, 2025.
- Wang, Y., Hu, M., Guo, S., Wang, Y., Zheng, J., Yang, Y., Zhu, W., Tang, R., Li, X., Liu, Y., Le Breton, M., Du, Z., Shang, D., Wu, Y., Wu, Z., Song, Y., Lou, S., Hallquist, M., and Yu, J.: The secondary formation of organosulfates under interactions between biogenic emissions and anthropogenic pollutants in summer in Beijing, *Atmos. Chem. Phys.*, 18, 10693–10713, <https://doi.org/10.5194/acp-18-10693-2018>, 2018.
- Wang, Z. B., Hu, M., Yue, D. L., Zheng, J., Zhang, R. Y., Wiedensohler, A., Wu, Z. J., Nieminen, T., and Boy, M.: Evaluation on the role of sulfuric acid in the mechanisms of new particle formation for Beijing case, *Atmos. Chem. Phys.*, 11, 12663–12671, <https://doi.org/10.5194/acp-11-12663-2011>, 2011.
- Wardlaw, D. M. and Marcus, R. A.: RRKM reaction rate theory for transition states of any looseness, *Chem. Phys. Lett.*, 110, 230–234, 1984.
- Wu, S., Dai, L. H., Wei, Y., Zhu, H., Zhang, Y. J., Schwab, J., and Yuan, C. S.: Atmospheric ammonia measurements along the coastal lines of Southeastern China: Implications for inorganic nitrogen deposition to coastal waters, *Atmos. Environ.*, 177, 1–11, 2017.

- Xing, Y. F., Xu, Y. H., Shi, M. H., and Lian, Y. X.: The impact of PM_{2.5} on the human respiratory system, *J. Thorac. Dis.*, 8, 69–74, 2016.
- Yang, Y., Liu, L., Wang, H., and Zhang, X.: Molecular-scale mechanism of sequential reaction of oxalic acid with SO₃: potential participator in atmospheric aerosol nucleation, *J. Phys. Chem. A*, 125, 4200–4208, 2021.
- Yao, L., Garmash, O., Bianchi, F., Zheng, J., Yan, C., Kontkanen, J., Junninen, H., Mazon, S. B., Ehn, M., Paasonen, P., Sipilä, M., Wang, M., Wang, X., Xiao, S., Chen, H., Lu, Y., Zhang, B., Wang, D., Fu, Q., Geng, F., Li, L., Wang, H., Qiao, L., Yang, X., Chen, J., Kerminen, V. M., Petäjä, T., Worsnop, D. R., Kulmala, M., and Wang, L.: Atmospheric new particle formation from sulfuric acid and amines in a Chinese megacity, *Science*, 361, 278–281, 2018.
- Yao, L., Fan, X., Yan, C., Kurtén, T., Daellenbach, K. R., Li, C., Wang, Y., Guo, Y., Dada, L., Rissanen, M. P., Cai, J., Tham, Y. J., Zha, Q., Zhang, S., Du, W., Yu, M., Zheng, F., Zhou, Y., Kontkanen, J., Chan, T., Shen, J., Kujansuu, J. T., Kangasluoma, J., Jiang, J., Wang, L., Worsnop, D. R., Petäjä, T., Kerminen, V. M., Liu, Y., Chu, B., He, H., Kulmala, M., and Bianchi, F.: Unprecedented ambient sulfur trioxide (SO₃) detection: possible formation mechanism and atmospheric implications, *Environ. Sci. Technol.*, 7, 809–818, 2020.
- Yin, R., Yan, C., Cai, R., Li, X., Shen, J., Lu, Y., Schobesberger, S., Fu, Y., Deng, C., Wang, L., Liu, Y., Zheng, J., Xie, H., Bianchi, F., Worsnop, D. R., Kulmala, M., and Jiang, J.: Acid-base clusters during atmospheric new particle formation in urban Beijing, *Environ. Sci. Technol.*, 55, 10994–11005, 2021.
- Zhang, H., Worton, D. R., Lewandowski, M., Ortega, J., Rubitschun, C. L., Park, J.-H., Kristensen, K., Campuzano-Jost, P., Day, D. A., Jimenez, J. L., Jaoui, M., Offenberg, J. H., Kleindienst, T. E., Gilman, J., Kuster, W. C., de Gouw, J., Park, C., Schade, G. W., Frossard, A. A., Russell, L., Kaser, L., Jud, W., Hansel, A., Cappellin, L., Karl, T., Glasius, M., Guenther, A., Goldstein, A. H., Seinfeld, J. H., Gold, A., Kamens, R. M., and Surratt, J. D.: Organosulfates as tracers for secondary organic aerosol (SOA) formation from 2-Methyl-3-Buten-2-ol (MBO) in the atmosphere, *Environ. Sci. Technol.*, 46, 9437–9446, 2012a.
- Zhang, H., Kupiainen-Määttä, O., Molinero, V., Zhang, Y., and Li, Z.: The enhancement mechanism of glycolic acid on the formation of atmospheric sulfuric acid-ammonia molecular clusters, *J. Chem. Phys.*, 146, 184308, <https://doi.org/10.1063/1.4982929>, 2017.
- Zhang, H., Li, H., Liu, L., Zhang, Y., Zhang, X., and Li, Z.: The potential role of malonic acid in the atmospheric sulfuric acid-ammonia clusters formation, *Chemosphere*, 203, 26–33, 2018.
- Zhang, H., Gao, R., Li, H., Li, Y., Xu, Y., and Chai, F.: Formation mechanism of typical aromatic sulfuric anhydrides and their potential role in atmospheric nucleation process, *J. Environ. Sci.*, 123, 54–64, 2023a.
- Zhang, H., Wang, W., Fan, L., Li, J., Ren, Y., Li, H., Gao, R., and Xu, Y.: The role of sulfur cycle in new particle formation: Cycloaddition reaction of SO₃ to H₂S, *J. Environ. Sci.*, 148, 489–501, 2025.
- Zhang, J. and Dolg, M.: Global optimization of clusters of rigid molecules using the artificial bee colony algorithm, *Phys. Chem. Chem. Phys.*, 18, 3003–3010, 2016.
- Zhang, Q., Wang, Y., Liu, M., Zheng, M., Yuan, L., Liu, J., Tao, S., and Wang, X.: Wintertime formation of large sulfate particles in China and implications for human health, *Environ. Sci. Technol.*, 57, 20010–20023, 2023b.
- Zhang, R., Khalizov, A., Wang, L., Hu, M., and Xu, W.: Nucleation and growth of nanoparticles in the atmosphere, *Chem. Rev.*, 112, 1957–2011, 2012b.
- Zhang, R., Wang, G., Guo, S., Zamora, M. L., Ying, Q., Lin, Y., Wang, W., Hu, M., and Wang, Y.: Formation of urban fine particulate matter, *Chem. Rev.*, 115, 3803–3855, 2015.
- Zhang, X., Lian, Y., Tan, S., and Yin, S.: Organosulfate produced from consumption of SO₃ speeds up sulfuric acid–dimethylamine atmospheric nucleation, *Atmos. Chem. Phys.*, 24, 3593–3612, <https://doi.org/10.5194/acp-24-3593-2024>, 2024.
- Zhao, B., Donahue, N. M., Zhang, K., Mao, L., Shrivastava, M., Ma, P.-L., Shen, J., Wang, S., Sun, J., Gordon, H., Tang, S., Foust, J., Wang, M., Gao, Y., Yan, C., Singh, B., Li, Z., Huang, L., Lou, S., Lin, G., Wang, H., Jiang, J., Ding, A., Nie, W., Qi, X., Chi, X., and Wang, L.: Global variability in atmospheric new particle formation mechanisms, *Nature*, 631, 98–105, 2024.
- Zheng, B., Tong, D., Li, M., Liu, F., Hong, C., Geng, G., Li, H., Li, X., Peng, L., Qi, J., Yan, L., Zhang, Y., Zhao, H., Zheng, Y., He, K., and Zhang, Q.: Trends in China’s anthropogenic emissions since 2010 as the consequence of clean air actions, *Atmos. Chem. Phys.*, 18, 14095–14111, <https://doi.org/10.5194/acp-18-14095-2018>, 2018.
- Zu, H., Zhang, S., Li, S., Liu, L., and Zhang, X.: The synergistic nucleation of iodic acid and sulfuric acid: A vital mechanism in polluted marine regions, *Atmos. Environ.*, 318, 120266, <https://doi.org/10.1016/j.atmosenv.2023.120266>, 2024a.
- Zu, H., Zhang, S., and Liu, L.: The vital role of sulfuric acid in iodine oxoacids nucleation: impacts of urban pollutants on marine atmosphere, *Environ. Res. Lett.*, 19, <https://doi.org/10.1088/1748-9326/ad193f>, 2024b.